ChemMedChem

Research Article
doi.org/10.1002/cmdc.202200444

Chemistry Europe
European Chemical Societies Publishing

www.chemmedchem.org

Special Collection

Biomolecular Interactions of Cytotoxic Ruthenium Compounds with Thiosemicarbazone or Benzothiazole Schiff Base Chelates

Sanam Maikoo,[a] Bheki Xulu,[a] Allen Mambanda,[a] Ntando Mkhwanazi,[b] Candace Davison,[b] Jo-Anne de la Mare,*[b] and Irvin Noel Booysen*[a]

Herein we illustrate the formation and characterization of new paramagnetic ruthenium compounds, *trans-P*-[RuCl(PPh$_3$)$_2$(pmt)]Cl (**1**) (Hpmt = 1-((pyridin-2-yl)methylene)thiosemicarbazide), *trans-P*-[RuCl(PPh$_3$)$_2$(tmc)]Cl (**2**) (Htmc = 1-((thiophen-2-yl)methylene)thiosemicarbazide) and a diamagnetic ruthenium complex, *cis-Cl*, *trans-P*-[RuCl$_2$(PPh$_3$)$_2$(btm)] (**3**) (btm = 2-((5-hydroxypentylimino)methyl)benzothiazole). Agarose gel electrophoresis experiments of the metal compounds illustrated dose-dependent binding to *g*DNA by **1**–**3**, while methylene blue competition assays suggested that **1** and **2** are also DNA intercalators. Assessment of the effects of the compounds on topoisomerase function indicated that **1**–**3** are capable of inhibiting topoisomerase I activity in terms of the ability to nick supercoiled plasmid DNA. The cytotoxic activities of the metal complexes were determined against a range of cancer cell lines versus a non-tumorigenic control cell line, and the complexes were, in general, more cytotoxic towards the cancer cells, displaying IC$_{50}$ values in the low micromolar range. Time-dependent stability studies showed that in the presence of strong nucleophilic species (such as DMSO), the chloride co-ligands of **1**–**3** are rapidly substituted by the former as proven by the suppression of the substitution reactions in the presence of an excess amount of chloride ions. The metal complexes are significantly stable in both DCM and an aqueous phosphate buffer containing 2% DMSO.

Introduction

Among the key design attributes for the next-generation of metal-based chemotherapeutic drugs is target specificity, which defines the capability of a drug to kill cancerous cells while being non-toxic to healthy tissue.[1] In particular, N-heterocyclic coordination compounds of ruthenium have sparked interest in the design of novel anti-cancer agents as these metal complexes could be potential substitute drugs for current established chemotherapeutic drugs with undefined biodistribution patterns.[2] In comparison to platinum-based anticancer pharmaceuticals, these leading ruthenium-containing chemotherapeutics exhibit comparable cytotoxicity but are more physiological compatible owing to ruthenium's similar properties to the essential metal, iron.[3]

A typical design strategy in organoruthenium drugs comprises of the use of biologically active chelators that can tailor the biodistribution patterns towards specific cancers.[4] This design approach has resulted in promising metal-based anticancer drugs which display good target specificity and the latter is induced by synergetic effects of the metal center and its bio-active chelating ligands.[5] Herein, we consider two prominent bio-active moieties (*viz.* benzothiazole and thiosemicarbazide) as potential pharmacophores, which were incorporated into multidentate Schiff bases.

Our selections are motivated by the fact that the benzothiazole group is a common synthon for numerous organic pharmaceuticals, whilst the derivatives of thiosemicarbazide are of considerable interest since they display a broad spectrum of biological activities, such as anti-viral and -cancer activities.[6] Moreover, ruthenium compounds with N-donor ligands encompassing either of these biologically active moieties (*viz.* thiosemicarbazide and benzothiazole), have shown enhanced *in vitro* anticancer activities compared with their free ligands.[7] In addition, the anticancer activities of this class of metal-based drugs can be readily modulated by their structures, *e.g.* the ruthenium(II) complex salt, *cis*-[Ru(bipy)$_2$(4,5′-bbtb)]$^{2+}$ (bbtb = *bis*-(benzothiazol-2-yl)-2,2′-bipyridine) interacts with CT-DNA *via* groove-binding due to the steric demands of its N-donor chelating.[8]

In this study, we report the formation and characterization of ruthenium(II) and -(III) compounds with Schiff bases with

[a] Dr. S. Maikoo, Dr. B. Xulu, Dr. A. Mambanda, Prof. I. N. Booysen
School of Chemistry and Physics
University of KwaZulu-Natal
Pietermaritzburg (South Africa)
E-mail: Booyseni@ukzn.ac.za
[b] N. Mkhwanazi, Dr. C. Davison, Dr. J.-A. de la Mare
Centre for Chemico and Biomedicinal Research
Department of Biochemistry and Microbiology
Faculty of Science,
Rhodes University
PO Box 94, Grahamstown 6140 (South Africa)
E-mail: j.delamare@ru.ac.za

Supporting information for this article is available on the WWW under https://doi.org/10.1002/cmdc.202200444

Special Collection *This article belongs to the Joint Special Collection "Biological and Medicinal Chemistry in Africa".*

benzothiazole or thiosemicarbazone moieties. These ruthenium compounds: *trans-P*-[$RuCl(PPh_3)_2$(pmt)]Cl (**1**), *trans-P*-[$RuCl(PPh_3)_2$(tmc)]Cl (**2**) and *cis-Cl, trans-P*-[$RuCl_2(PPh_3)_2$(btm)] (**3**) were isolated from the coordination reactions of *trans*-[$RuCl_2(PPh_3)_3$] with the Schiff bases 1-((pyridin-2-yl)methylene)thiosemicarbazide (Hpmt), 1-((thiophen-2-yl)methylene)thiosemicarbazide (Htmc) and 2-((5-hydroxypentylimino)methyl)benzothiazole (btm), respectively. We have also probed the interaction of the metal compounds with human genomic DNA (gDNA) and bovine serum albumin (BSA), as well as studied their radical scavenging abilities, topoisomerase inhibitory activity and cytotoxicity against various cancerous cell lines in comparison to a non-cancerous cell line.

Results and Discussion

Formation, spectroscopic and redox data of 1–3

The ruthenium compounds **1** and **2** were isolated in moderate yields from respective equimolar coordination reactions of *trans*-[$RuCl_2(PPh_3)_3$] with Hpmt and Htmc, whilst a 1:1 molar reaction with btm resulted in the isolation of metal complex **3** in low yield. In the case of **1** and **2**, both their Schiff base chelators coordinate as monoanionic tridentate chelators *via* their $S_{thiolate}N_{imino}N_{pyridine}$ (in **1**) $S_{thiolate}N_{imino}S_{thiophene}$ (in **2**) donor sets. Numerous ruthenium complexes with thiosemicarbazone Schiff bases have shown preferential coordination modes through their imino nitrogen and thiolate sulphur donor atoms, *e.g.* [$Ru(CO)Cl(PPh_3)_2(TSC^{N-S})$] ($TSC^{N-S}$ = 1-((thiophen-2-yl)methylene)thiosemicarbazide).[9] In fact, thiosemicarbazone ligands can exist in different tautomeric forms; as a thione tautomer or in the thiol forms, refer to see Scheme 1. Therefore, as per literature trends, thiosemicarbazone ligands can function as neutral tridentate chelators in the thione form or anionic chelators in the thiolate forms.[9–10]

In **3**, the btm chelator functions as a neutral bidentate chelator *via* the $N_{imino}N_{benzothiazole}$ donor set, which corresponds well with trends found within literature. In particular, ruthenium compounds with benzothiazole moieties have shown tendencies in coordination affinity, whereby the $N_{benzothiazole}$ donor atom bonds to soft acceptor metal centers such as ruthenium(II). An example of this phenomenon is the diamagnetic ruthenium compound, [Ru(pybs)$(PPh_3)(CH_3CN)_2$Cl]Cl (pybs = 2-(2-pyridyl)benzothiazole).[10–11] Furthermore, the metal compounds **1–3** are stable in air, soluble in chloroform, dichloromethane, dimethyl sulfoxide and tetrahydrofuran, as well as partially soluble in alcoholic media and acetonitrile.

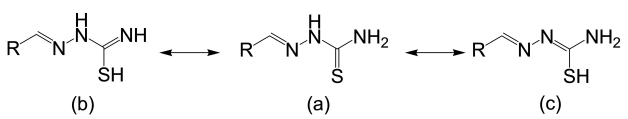

Scheme 1. Tautomers of thiosemicarbazone: (**a**) thione, (**b**) thiol form 1 and (**c**) thiol form 2.

The ^{1}H NMR spectrum of the diamagnetic metal complex **3** is dominated by a multiplet within the region 7.50–7.10 ppm, which is partly owing to the triphenylphosphine co-ligands,[12] see Figure S1. Evidence of coordination through the imino nitrogen arises from a significant shift of its singlet (8.64 ppm in the proton spectrum of the free ligand) which now forms part of the multiplet region (7.50–7.10 ppm).[13] It is evident that the signals for the protons of the benzothiazole moiety (*viz. H2, H3, H4, H5)* clearly show noteworthy changes upon coordination. More specifically, a multiplet between 8.21–8.11 ppm (for *H2* and *H5*) within the free-ligand's proton spectrum splits into two individual doublets (at 8.19 and 8.04 ppm) in the proton spectrum of **3**, while the remaining benzothiazole protons, which originally formed part of the intense multiplet between 7.60–7.50 ppm (for *H8* and *H9*), coalesce into the multiplet region between 7.50–7.10 ppm as observed in the ^{1}H NMR spectrum of **3**. This is indicative of the change in the electronic environment around the benzothiazole moiety post coordination. Similarly, the aliphatic protons coalesce into two broad, poorly resolved signals. The magnetic equivalence of the *trans*-axial phosphorous atoms was confirmed by the presence of a single peak in the ^{31}P NMR spectrum,[14] see Figure S2.

Indicatively, as shown in their NMR spectra, the Ru–P bonds' infrared stretches distinctively appear between 691 and 742 cm^{-1}, which occur in the same wavenumber region [746–522 cm^{-1}] as other ruthenium Schiff bases stabilized by *trans*-$[Ru(PPh_3)_2]^+$ cores, see Figure S3.[15] The respective imino vibrational bands of **1**–**3** occur at 1552, 1579 and 1534 cm^{-1}, whereas the solid-state IR spectra of the free thiosemicarbazone ligands (Hpmt and Htmc) show medium to strong vibrational bands at 1603 cm^{-1} (for Hpmt), 1595 cm^{-1} (for Htmc) and 1636 cm^{-1} (for btm); due to the stretches of the imine bonds.[16] Typically, upon coordination of the Schiff bases, their imino stretches appear at lower wavenumbers with respect to the free Schiff bases and are associated with coordination *via* the imino nitrogen donor atoms.[17]

As mentioned before, thiosemicarbazone ligands can exist in different tautomeric forms; a thione or thiol forms. Therefore, as per literature trends, thiosemicarbazone ligands can function as neutral tridentate chelators in the thione form or anionic tridentate chelators in the thiolate forms.[9,17] The IR bands appearing at 1229 and 1274 cm^{-1} within the spectra of the free ligands, Hpmt and Htmc are ascribed to the vibrations of the C=S bonds. However, these vibrational bands are not present in the solid-state IR spectra of **1** and **2**, while new IR stretches at 1586 (for **1**) and 1608 cm^{-1} (for **2**) ascribed to the $\nu(C{=}N)_{thiolate}$ bonds are evident. Consequently, the latter provides evidence of the conversion of Hpmt and Htmc to their respective thiolate forms prior to coordination. The amido bonds are found as weak intensity bands at 3468, 3049 cm^{-1} for **1** and 3353, 3048 cm^{-1} for **2**, while a medium-intensity of **3** at 3461 cm^{-1} is accounted to the alcohol vibration. Furthermore, the $\nu(C{=}N)_{imino}$ and $\nu(C{=}N)_{benzothiazole}$ signals of **3** appear at 1566 and 1484 cm^{-1}.

Electronic spectra of the metal compounds were recorded in a non-coordinative solvent, dichloromethane at room temperature, see Figures S4–S6. All the metal compounds exhibited intense π-π^* intraligand transitions below 300 nm

while the charge electronic transitions observed in the region 308–533 nm are attributed to charge-transfer (CT) bands.[18] The electronic spectra of the paramagnetic complexes **1** and **2** (d^5, $S=^1/_2$) display broad absorption bands at 481 nm and 447 nm respectively, due to their ligand-to-metal charge transfers (LMCTs) resulting from the molecular orbitals of the chloro co-ligands and Schiff base chelators, to the partially filled d^5 orbital of the Ru^{III} complexes. The electronic spectrum of **1** also shows a shoulder at 680 nm (see Figure S6 inset) which is recognized as a *d-d* transition, congruent with low-spin octahedral geometry.[19] In the diamagnetic complex **3** (d^6, $S=0$), the absorption band present at 531 nm is assignable to Ru(II)-to-ligand metal-to-ligand charge transfer (MLCT).[19]

Solid and liquid samples were used to collect the low-temperature EPR data for **1** and **2**, see Figures 1 and **S7**. The solid state EPR spectra of both metal compounds show three distinctive signals with different *g*-values (*viz.* $g_x \neq g_y \neq g_z$), signifying the presence of magnetic anisotropy and rhombic distortion of their octahedral geometries, refer to Table 1. For the solutions of **1** and **2**, single isotropic signals were attained due to faster relaxation lifetimes of their spins. Collectively, the *g*-values obtained were comparable to other low-spin d^5 ruthenium compounds with distorted octahedral geometries.[20] For example, a g-value (g_{iso}) = 2.3 was attained for the solution of *trans*-$[RuCl_4(H_2mtpO)(dmso)]\cdot 4H_2O$ (HmtpO = 5-methyl-1,2,4-triazolo[1,5-*a*]pyrimidin-7-(4*H*)-one) while different *g*-values (*viz.* $g_x \neq g_y \neq g_z$) = 3.20, 2.75 and 1.75, respectively) were reported for the solid-state sample of $[(CH_3)_2NH_2]$*trans*-$[RuCl_4(HmtpO)_2]$.[20]

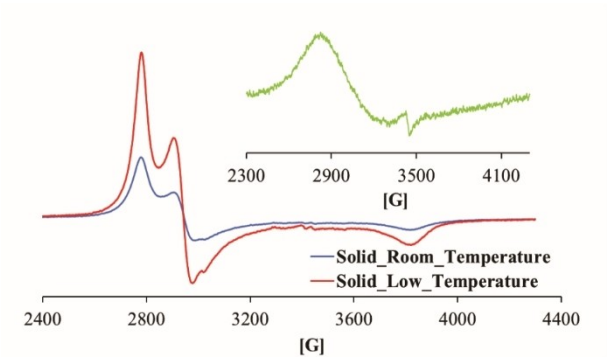

Figure 1. ESR spectra of **1** collected in the solid state at room (at 298 K) and low (at 77 K) temperatures. **Inset**: An identical ESR spectrum attained for the liquid samples collected at the two different temperatures.

Table 2. Selected CV parameters of **1**–**3** recorded in DCM at 100 mV/s.

Compound	1		2	3	Ferrocene
	I	II			
E_{pa} (V)	0.64	0.94	0.69	0.36	
E_{pc} (V)	0.56	0.81	0.51	0.28	
ΔE_p (mV)	80	130	180	80	90
$E_{1/2}$ (V)	0.60	0.88	0.60	0.32	0.50

The cyclic voltammogram (CV) of **1** showed two redox couples labelled **I** ($E_{1/2}$ = 0.60 V *vs* Ag | AgCl) and **II** ($E_{1/2}$ = 0.88 V *vs* Ag | AgCl), see Figure S8 and refer to Table 2. These are ascribed to metal-based redox processes as the CV of the free-ligand (Hpmt) did not show any redox activity within the same potential window. Redox processes **I** and **II** are assigned to the Ru(III)/ Ru(II) and the Ru(III)/ Ru(IV) redox couples, respectively. However, the CV of **2** contains a single quasi-reversible redox couple I ($E_{1/2}$ = 0.60 V *vs* Ag | AgCl), see Figure S9. This is assigned to the Ru(III)/ Ru(II) redox couple. The Ru(III)/Ru(IV) redox couple (due to the d^5-d^6 interconversion of **3)** appears at a lower halfwave potential of 0.32 V *vs* Ag | AgCl, see Figure S10.[21] As expected, these diffusion-controlled redox processes afforded singular (for **2** and **3**) and dual (for **1**) symmetrical peaks within their respective SWVs. The aforementioned redox assignments are made based on the comparative redox potentials to other cyclometallated monomeric ruthenium compounds More specifically, voltammetry analysis of a dimethyl sulfoxide solution of the paramagnetic complex, [*bis*-salicylaldehyde-4(*N*)-ethylthiosemicarbazone)(triphenylphosphino)ruthenium(III)] and [Ru(Sal-etsc)(H-Sal-etsc)(PPh_3)], illustrated a halfwave potential of 0.602 V (*vs* Ag | AgCl) accounted to the Ru(III)/ Ru(II) redox couple within the non-coordinative solvent, dichloromethane.[21a] In addition, all CVs exhibit quasi-reversible behaviour since their peak-to-peak separations are higher than that of the standard ferrocene, refer Table 2 and Figure 2.

As per literature trends, **1** showed a potential difference of 1.48 V. between its metal-based redox couple, which is comparable to the paramagnetic complex, [Ru^{III}(Sal-etsc)(H-Sal-etsc)(PPh_3)] (H-Sal-etsc = salicylaldehyde-4(*N*)-ethylthiosemicarbazone) for which the Ru(III)/Ru(IV) and Ru(III)/Ru(II) redox couples appeared at 0.602 V and −0.609 V (*vs* Ag | AgCl), respectively. Likewise, a series of *ortho*-metallated ruthenium(III) complexes comprising of Schiff bases derived from benzaldehyde and acid hydrazides (H_2L), display Ru(III)/Ru(IV) oxidation couples within the potential range of 0.35–0.98 V (vs. Ag | AgCl)

Table 1. Selected ESR spectral data of **1** and **2** at room and low temperatures.

Sample	State	Temperature	g_x	g_y	g_z	g_{iso}
1	Solid	77 K	2.52	2.38	1.83	–
		298 K	2.53	2.38	1.83	–
	Liquid	77 K	–	–	–	2.28
		298 K	–	–	–	2.27
2	Solid	77 K	2.24	2.10	1.98	–
		298 K	2.43	2.18	1.91	–
	Liquid	77 K	–	–	–	2.27
		298 K	–	–	–	2.38

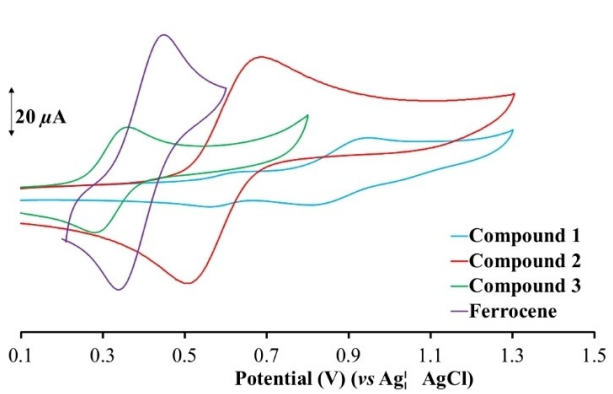

Figure 2. Overlay CVs of **1**–**3** and ferrocene (at 100 mV/s) in dichloromethane.

in dichloromethane.[21b] In addition, analogues of the diamagnetic ruthenium complexes, $[RuCl_2(PPh_3)_2(N)_2]$ and $[RuCl_2(PPh_3)_2(N–N)]$ (where N = pyridine derivatives and N–N = phenanthroline or bipyridine derivatives) showed a synonymous redox couple to **3**, where similar half-wave potentials between 0.3 and 0.4 V were attained..[22]

Crystallographic descriptions of 1–3

Coordination behaviours of the individual Schiff bases chelators induce the formation of constrained 5-membered rings within the corresponding basal planes of **1–3**, which renders octahedral distortions given by their individual bite angles [N2–Ru–N1 = 77.74(15)°, N2–Ru–S = 83.19(2)° for **1**, N1–Ru–S2 = 78.7(1)°, N1–Ru–S1 = 82.2(1)° for **2** and N1–Ru–N2 = 78.2(3)° for **3**] all of which deviate from the ideal equatorial bond angle of 90°, see Figure 3. In turn, the respective constrained bite angles of **1** and **2** rationalize the N1–Ru–Cl1 [178.42(12)°], N1–Ru–S [160.93(10)°] for **1** and S1-Ru–S2 [160.01(4)°], N1–Ru–Cl1 [177.8(1)°] for **2** are non-linear while the opposing bond angle [Cl1–Ru–Cl2 = 90.17(7)°] (with regard to the bite angle of **3**) is essentially equal to 90° but the neighbouring bond angles [Cl1–Ru–N1 = 100.2(2)° and Cl2-Ru–N2 = 91.5(2)°] differ from the aforementioned idealized bond angle.

The Ru–P bonds are comparable to those of other ruthenium(II) and –(III) Schiff base complexes with *trans-axial* triphenylphosphine co-ligands.[23] In addition, the ruthenium-to-halide bonds of **1** [Ru–Cl1 = 2.4289(11) Å] and **2** [Ru–Cl1 = 2.421(1) Å] are shorter than those of **3** [Ru–Cl1 = 2.435(2) Å and Ru–Cl2 = 2.448(2) Å], which emphasizes the higher Lewis acidic characters of the paramagnetic metal centers of **1** and **2**. Variable *trans*-influence is imposed on the chloride co-ligands of **3** by its imino and benzimidazole nitrogens, which result in Ru–Cl distances that differ. The $Ru–S_{thiolate}$ bond lengths of 2.3812(12) for **1** and 2.345(1) Å for **2** are similar to those of other ruthenium thiosemicarbazones where coordination occurs *via* the chelating ligands neutral imino nitrogens and deprotonated thiolate sulfurs. For instance, the dimeric ruthenium(III) compound, $(\mu\text{-}S)_2[(H_2nptsc)_2]$ (H_2nptsc = 1-((2-hydroxynaphthalen-3-yl)methylene)thiosemicarbazide) had respective Ru–S distances of 2.250(5) and 2.262(6) Å, while the analogous bonds of the diamagnetic ruthenium(II) compounds, $[Ru(H\text{-}Sal\text{-}tsc)(CO)Cl\text{-}(PPh_3)_2]$ (H-Sal-tsc = salicylaldehydethiosemicarbazone) and $[Ru(Sal\text{-}tsc)(CO)(PPh_3)_2]$ are 2.4012(7) and 2.344(2) Å, respectively.[24] Similarly, the ruthenium(III) to imino nitrogen bonds of **1** [Ru–N2 = 1.970(4) Å] and **2** [Ru–N1 = 2.039(4) Å] compare well with those [1.962(15) and 2.062(15) Å] of the aforementioned paramagnetic ruthenium compound. Metal coordination to the sp^2-benzothiazole nitrogen donor of **3** affords a Ru–N1 bond length of (2.089(6 Å), which is essentially equal to the $Ru–N_{benzothiazole}$ bond length of 2.079(2) Å for the $[RuCl(obs)_2(PPh_3)]$ (Hobs = 2-hydroxyphenylbenzothiazole), while the $Ru–N_{imino}$ bond of **2** and the $Ru–N_{pyridyl}$ bonds are in accordance with bond distances of ruthenium(II) compounds with 2-((pyridin-2-yl)methyleneamino) moieties.[25]

The mutual tautomeric forms of the pmt and tmc chelators can be unequivocally established when comparing their thiolate bonds [C7–S = 1.703(5) Å for **1** and C4-S2 = 1.721(5) Å for **2**] with that of the intracyclic C–S bonds [C7-S = 1.726(8) Å and C1-S = 1.724(9) Å] of **3**. In addition, the shorter C7–N4 [1.331(6) Å] than C7-N3 [1.357(6) Å] of **1** suggest double bond character for the former. These double bond lengths are similar to the intracyclic C=N in pyridine [C5–N1 = 1.337(6) Å and C1-N1 = 1.338(6) Å]. However, the C6–N3 bond was found to be longer than the C6-N2 bond, which implies that *pi*-delocalization occur throughout the N3 C6 N2 N1 aliphatic moiety. Evidently, the intraligand N–N bonds of **1** [1.368(6) Å] and **2** [1.380(6) Å] differs. The localized imino bonds are also comparable [C6-N2 = 1.305(6) Å for **1**, C5–N1 = 1.298(7) Å for **2** and C8–N2 = 1.30(1) Å for **3**].

Antioxidant studies

Abnormal oxidative stress is a substantial contributor to the onset of numerous non-communicable diseases, such as cancers and inflammatory conditions.[26] Hence, complementary synthetic drugs with high efficacies are required to supplement the body's natural defense mechanisms by scavenging for the reactive oxygen species (ROS) within the blood stream.[27] Organoruthenium species have sparked interest as metal-based antioxidants, whereby their mechanism of activities to retard oxidative damage is hypothesized to be co-dependent on the metal's redox properties and the ligands' propensity to quench the radicals either by proton donation or a recombination reaction with the ROS.[28] In this study, the radical scavenging capabilities of **1**–**3**, against the DPPH and NO radicals were studied and compared to the *in vitro* antioxidant activities with the standard, vitamin C. The 50% inhibitory concentration (IC_{50}) values of the metal compounds (Table S1) vary from 44 to 85 μM against the DPPH radical and from 27 to 64 μM against the NO radical. It suggests that the ruthenium complexes displayed significantly higher antioxidant activities in comparison to the natural antioxidant, vitamin C.

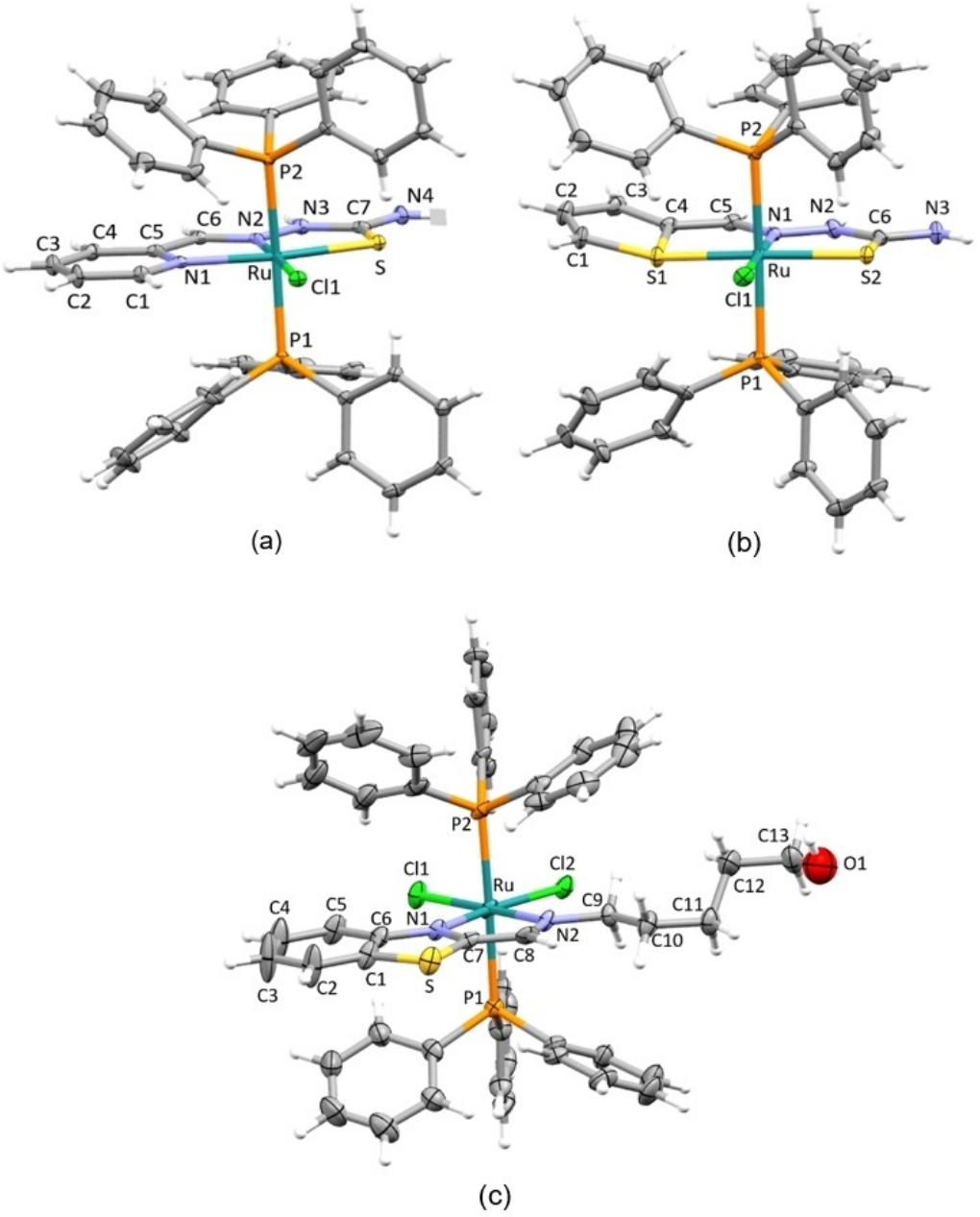

Figure 3. ORTEP view of compounds showing 50% probability displacement ellipsoids and the atom labelling. The solvent molecules of recrystallization and counterions have been omitted. (a) Compound **1**, (b) Compound **2**, (c) Compound **3**.

DNA interaction studies

Agarose gel electrophoresis (AGE) experiments using human genomic DNA (*g*DNA) were performed with **1**–**3** to ascertain their CT-DNA binding capabilities. In this assay, a decrease in band intensity (and not necessarily band position) on the agarose gel indicates that the compounds can compete with and displace ethidium bromide to bind to the gDNA. AGE image analysis illustrates that the metal complexes display concentration-dependent binding to *g*DNA, see Figure 4. Relative to the negative control (DMSO, -), decreases in the intensity of the EtBr stained gDNA are observed for the lanes of **1** and **2**, at lower concentrations. In addition, higher concentrations of **1** and **3** demonstrated a considerable dose-dependent reduction in intensity of the EtBr-stained DNA bands. Based on the aforementioned visual observations, it can be concluded that **1–3** are able to displace the DNA intercalator, EtBr. This is consistent with previous reports of the binding modes of ruthenium compounds to CT-DNA and human gDNA as deduced by DNA-ethidium bromide competition studies.[29]

To further confirm whether **1**–**3** were DNA intercalators and to determine their mode of interaction, a quantitative, competitive DNA binding methylene blue assay was utilised, see Figure 5. Methylene blue is a verified fluorescent DNA inter-

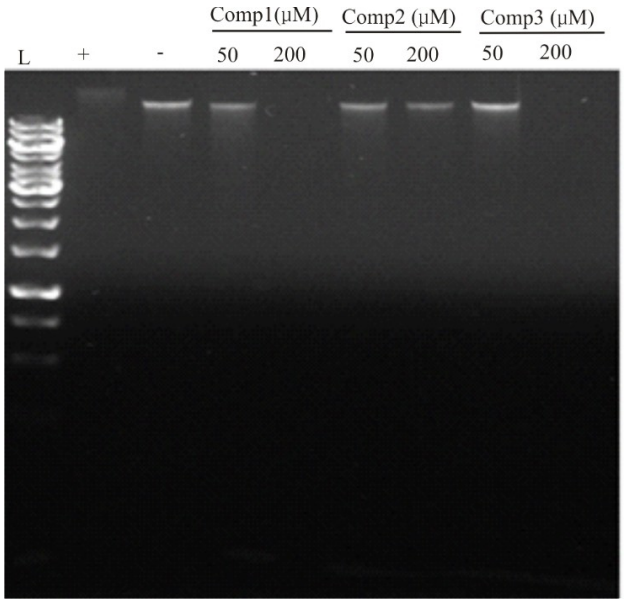

Figure 4. Assessment of binding of compounds **1**–**3** to human genomic DNA by agarose gel electrophoresis. Image of 0.8 % agarose gel stained with 0.5 μg/μL ethidium bromide used to analyze compounds **1**–**3** incubated with gDNA. Lane 1: Thermo Scientific Gene-Ruler 1 Kb, Lane 2: cisplatin control (+), Lane 3: DMSO control (−), Lane 4: Compound **1** (50 μM), Lane **5**: Compound **1** (200 μM), Lane 6: Compound **2** (50 μM), Lane 7: Compound **2** (200 μM), Lane 8: Compound **3** (50 μM, Lane 9: Compound **3** (200 μM).

calator. A fixed amount of calf thymus DNA was combined with the dye in the presence or absence of the complexes **1**–**3**, with 0.05 % (v/v) DMSO as vehicle control. Methylene blue displays a strong fluorescence emission in the range of 660–670 nm, however a decrease in fluorescence intensities is observed when methylene blue complexes with DNA, which is directly related to the reduction of free methylene blue molecules in the medium.[30] It can be noted from Figure 5, that **1** (Figure 5A), and **2** (Figure 5B) competitively bind to the calf thymus DNA in a concentration-dependent manner, as observed by the increase in the fluorescence intensity relative to that of the DNA or compounds alone, or the DMSO vehicle control. Compound **3** appears to have no effect on the ability of methylene blue to bind to the DNA and it can be suggested from these results that it is not a DNA intercalator. DNA intercalation ability of ruthenium compounds is well established The most widely reported intercalators are the Ru(II) polypyridyl complexes, such as $[Ru(bpy)_2(dppz)]^{2+}$ (bpy = 2,2′-bipyridine, dppz = dipyridophenazine). The latter complex was developed as a luminescent DNA probe and interacts strongly with DNA exclusively *via* intercalation.[31]

The topoisomerase 1 (Topo I) inhibition assay assessed whether the complexes **1**–**3** interfere with the ability of Topo I to relax supercoiled DNA, see Figure 6. Topo I generates single strand nicks in DNA, initiating relaxation of the supercoiled conformation of plasmid DNA and decreasing the migration of the DNA through the agarose gel.[32] Figure 6 shows the supercoiled plasmid conformation, linearized plasmid (generated by restriction enzyme digestion) and plasmid DNA nicked by Topo I in lanes 1–3, respectively. It can be observed that compounds **1** (lanes 4 and 5) and **2** (lane 6 and 7) inhibited Topo I activity, returning the plasmid to the supercoiled conformation. However this effect was dose-dependent only in the case of compound **1**.

The inhibition was not, however complete, as indicated by the two distinct bands which were observed that correlated to the supercoiled DNA (lane 1), digested plasmid (lane 2) and untreated Topo 1 and plasmid DNA (lane 3). Compound **3**, on the other hand, appeared to cause complete inhibition of Topo I at 50 μM (lane 8), with only the supercoiled conformation being detected. The inhibitory effects of the compounds in terms of Topo I activity were superior to that of the known Topo I inhibitor, camptothecin,[33] which failed to inhibit the enzyme, even at the high concentration of 200 μM, in this assay (Lane 10). These findings are in line with other reports of the inhibition of topoisomerase I by ruthenium complexes.[34]

BSA interaction studies

Serum albumin is one of the major protein components of blood plasma and plays an integral role in the *in vivo* transport of pharmaceuticals in the blood stream. Consequently, the study of the binding properties of potential medicinal drugs towards serum albumin is of great importance in drug discovery. In this regard, the binding properties of BSA have been broadly studied due to its structural homology with human serum albumin. Ideally, to function as an transporter, a protein should maintain its structural features as much as possible upon binding with a drug.[35] In its native state (folded), BSA consists of three globular domains (**I**, **II** and **III**), which are subdivided into two smaller subdomains (**A** and **B**). Known binding sites for metal-based and organic compounds are typically the subdomains **IIA** and **IIIA** (known as sites **I** and **II**).[36] Well-defined electronic transitions in the UV-Visible absorption and fluorescence spectra of BSA are due to its tryptophan amino acid residues and any changes in the BSA protein can result in signal variations in the spectroscopic fingerprint observed.[37]

From the analysis of the BSA UV-Vis absorption spectra, it can be generally seen that with an increase in the concentration of a metal compound, slight blue shifts and distinct hypochromism are observed, see Figures S11–S13. These UV-Vis spectral changes are indicative of conformational changes in the BSA structure and changes in the polarity around the tryptophan residue. The observations suggest that the metal compounds stabilize the BSA structure upon binding, which results in a promotion of folding of the BSA strand, thereby masking the tryptophan residue within its hydrophobic pocket.[37–38] The apparent association constants (k_{app}) were calculated to be $9.02\times10^4\ M^{-1}$, $6.11\times10^4\ M^{-1}$ and $1.89\times10^4\ M^{-1}$, respectively. The binding affinity towards BSA must be strong enough to carry out transportation but also low enough to ensure that the metal compound is eventually released to the pharmacological targets. These metal compounds are therefore considered to be strong binders towards BSA as they

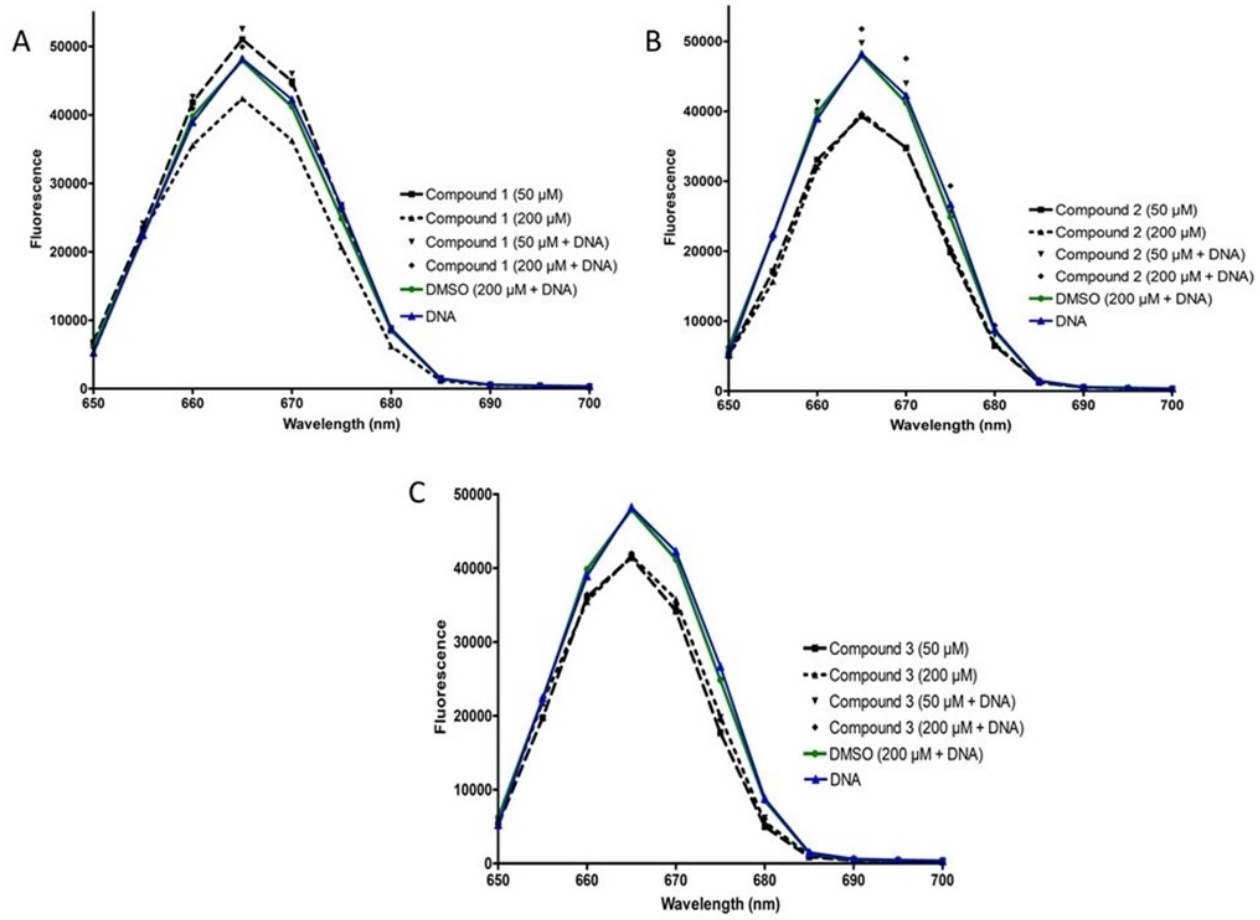

Figure 5. Methylene Blue Competition Assay to assess DNA intercalation ability of compounds **1–3**. Binding of (A) Compound **1**, (B) **2** and (C) **3** (50 and 200 μM) to 100 ng calf thymus DNA was assessed by an increase in methylene blue (15 μg/mL) fluorescence from 650–680 nm.

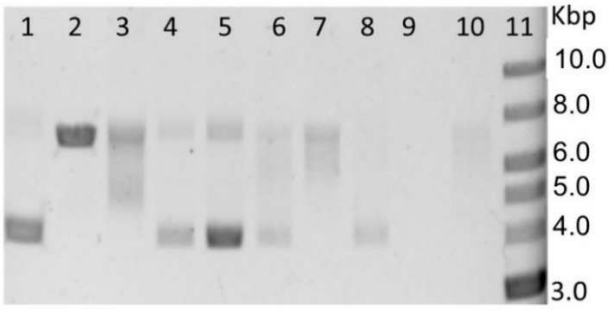

Figure 6. Assessment of inhibition of topoisomerase 1 by compounds **1**–**3**. Lane 1: Supercoiled pcDNA plasmid (pcDNA-CL8D-HisCYP2 A6 plasmid DNA alone), Lane 2: linearized plasmid DNA (digested with HindIII), Lane 3–10: plasmid DNA + topoisomerase I. Lane 3: untreated, Lane 4: Compound **1** (50 μM), Lane 5: Compound **1** (200 μM), Lane 6: Compound **2** (50 μM), Lane 7: Compound **2** (200 μM), Lane 8: Compound **3** (50 μM), Lane 9: : Compound **3** (200 μM), Lane 10: camptothecin, Lane 11: DNA ladder (New England Biolabs NO55OS 1 kb).

fall within the concentration range of other confirmed binders (10^4–10^6 M^{-1}).[39]

To corroborate the research findings of the electronic spectrophotometric study, fluorescence quenching of BSA, incurred by each of the metal compounds, was monitored. Indicatively, alterations in the fluorescence profile of BSA can be directly correlated to conformational changes in the BSA structure by detecting changes in the microenvironment of the tryptophan chromophore.[39] Figures S15–S17 illustrate the emission spectral effects of subsequent additions of standardized aliquots of the individual metal compounds to BSA. It is clearly seen that the characteristic emission band of BSA (due to the tryptophan residue) decreases progressively during each titration, which supports the formation of the metal compound-BSA adducts. In addition, a minor blue shift accompanied the latter spectral alterations within the BSA fluorescence spectra, which is synonymous of the tryptophan residues being enclosed in a hydrophobic pocket due to increased folding of the BSA strand (consistent with the results in the UV-Vis study).[36a,40]

This research data substantiates that the increased BSA folding occurs as a result of hydrogen bonding or Van der Waals contact during the interaction of the metal compounds with BSA within its hydrophobic subdomain **IIA**.[41] From their Stern-Volmer plots, the Stern-Volmer constants (K_{SV}) and quenching rate constants (k_q) were calculated (see Table 3).

Table 3. Binding parameters of **1–3** from BSA fluorescence experiments.

Compound	No Site marker		Ibuprofen		Warfarin	
	K_{SV} (M^{-1})	k_q ($M^{-1}s^{-1}$)	K_{SV} (M^{-1})	k_q ($M^{-1}s^{-1}$)	K_{SV} (M^{-1})	k_q ($M^{-1}s^{-1}$)
1	8.84×10^4	8.84×10^{12}	1.36×10^3	1.36×10^{11}	2.09×10^3	2.09×10^{11}
2	8.04×10^4	8.04×10^{12}	1.14×10^3	1.14×10^{11}	1.63×10^3	1.63×10^{11}
3	6.95×10^4	6.95×10^{12}	9.13×10^3	9.13×10^{11}	1.29×10^3	1.29×10^{11}

Static quenching of BSA as induced by the metal complexes was confirmed by the obtained k_q values. The latter is also supported by the characteristic UV-Vis spectral changes in the UV-Vis profile of BSA upon addition of the individual metal compounds.[36c,40a,42] Other ruthenium compounds in literature have reported similar K_{SV} and k_q values, *e.g.* the ruthenium(II) compounds, $[Ru(bpy)_2smp](PF_6)$ (bpy = 2,2′-bipyridine, smp = sulfamethoxypyridazine) and [Ru(η^6-*p*-cymene)(diclo)Cl] (Hdiclo = 2-[(2,6-dichlorophenyl)amino]benzeneacetic acid) possessed K_{SV} values of $1.02\times10^5\ M^{-1}$ and $6.45\times10^4\ M^{-1}$, respectively.[43]

Fluorescence spectroscopy is a useful tool in the method of site marker fluorescence probes to investigate the nature of binding sites and their affinities for different compounds.[44] Warfarin and Ibuprofen were utilized as site markers for sites **I** and **II**, respectively. The quenching of BSA by the metal compounds in the presence of each site marker was followed and the K_{SV} values determined as well as compared to the K_{SV} value obtained in the absence of the site markers, see Figures S18–S20. Table 3 shows the K_{SV} values of the metal compounds in the presence of the different site markers. The respective K_{SV} of the BSA-containing systems with both site markers decrease by the same order, relative to the systems in the absence of the site markers. These observations relate to the fact that the metal compounds displace both site markers and therefore have the ability to bind to both sites I and II within BSA.[44]

In vitro anticancer activity

A resazurin assay was performed to assess the anti-proliferative properties of **1**–**3** against various cancer cell lines, compared to a non-tumorigenic/non-cancerous cell line, using the commonly used chemotherapeutic drug paclitaxel (Ptx) as a positive control, refer to Table 4. In comparison to Ptx, which displayed low nanomolar IC_{50} values (ranging from 2.40–3.92 nM), the metal complexes were less toxic to the cancer cells, displaying IC_{50} values in the low micromolar range in general (ranging from 2.41–16.13 μM), with the exception of **1**, which displayed an IC_{50} value of 75.50 ± 1.16 μM against HCC70 breast cancer cells. In terms of selectivity for the cancer cell lines (HeLa cervical cancer, HCC70 triple negative breast cancer and MCF-7 hormone responsive breast cancer) over the non-cancerous control cell line MCF-12A, Ptx was 4- to 7-fold more toxic to the cancer cells (SI values from 4.12–6.73). The same trend, overall, was observed for **1–3**, which were 4- to 15-fold more toxic to the cancer cell lines than the MCF-12A cell line (SI values from 3.72–15.40), with the exception of **1**, which was more toxic to the MCF-12 A control cell line than the HCC70 cancer cell line (SI = 0.80). In some cases, the selectivity of **1**–**3** for the cancer cells compared to the non-cancerous cells was greater than that of paclitaxel, for example, the selectivity of **1** for MCF-7 breast cancer cells (SI = 11.55) and **2** for HeLa cells (SI = 15.40).

Triple negative breast cancers are more aggressive and have a poor prognosis, with no effective, standardized therapies currently available to treat this sub-type of the disease, since it is resistant to the hormonal therapies used to treat Luminal A cancers, represented by the MCF-7 cell line in this study.[45] In agreement with the results of this study, N-donor heterocyclic ruthenium compounds have previously been reported to

Table 4. Cytotoxicity analysis of the metal complexes (in μM) against cancer and non-cancerous cell lines.

Compound	HeLa (IC_{50} [μM] and SD) R^2	HCC70 (IC_{50} [μM] and SD) R^2	MCF-7 (IC_{50} [μM] and SD) R^2	MCF-12A (IC_{50} [μM] and SD) R^2
1	16,13 ± 1,08	75,50 ± 1,16	5,20 ± 1,058	60,05 ± 1,32
	0,9903	0,9424	0,9971	0,8389
	SI = 3.72	SI = 0.80	SI = 11.55	
2	2.41 ± 1,.04	6.26 ± 1.06	9′26 ± 1.08	37.12 ± 1.08
	0,9970	0.9949	0,9882	0.9912
	SI = 15.40	SI = 5.93	SI = 4.01	
3	6.29 ± 1.10	9′51 ± 1′10	8.87 ± 1.12	36.54 ± 1.08
	0,9903	0,9800	0.9775	0.9875
	SI = 5.81	SI = 3.84	SI = 4.12	
Paclitaxel (nM)	2.70 ± 1,12	3.92 ± 1.03	2.40 ± 1.11	16.16 ± 1.08
	0,9620	0.9920	0.9743	0.9877
	SI = 5.96	SI = 4.12	SI + 6.73	

exhibit anti-proliferation activities against TNBC cells.[46] However, the aforementioned ruthenium compounds exhibited predominately lower activities than **1**–**3** emphasizing the influence of their Schiff base chelators. Indicatively, metal complex **2** and **3** were more potent than the carbohydrazide Schiff base ruthenium(III) complexes: *cis-Cl*, *trans-P*-$[Ru^{III}Cl_2(carboim)(PPh_3)_2]$ (carboim = bpc, ttc or tpc) (Hbpc = *N*-[1,3-benzothiazole-2-ylmethylidene]pyridine-2-carbohydrazide, Httc = *N*-((uracil-5-yl)methylene)thiophene-2-carbohydrazide and Htpc = *N*-[(uracil-5-yl)methylidene]pyridine-2-carbohydrazide).[47] Consequently, this illustrates that the nature of the pharmacophores and the stereo-electronic properties of Schiff base ligands dictated their anticancer activities.

Furthermore, a ruthenium(III) complex, $[Ru(CO)(PPh_3)_2(L^a)]$ (H_2L^a = 2,4-dihydroxybenzaldehyde-S-methyldithiocarbazate) showed time-correlated apoptotic activities against MCF-7 cells (41.16 μM and 33.14 μM after 1 to 2 days) which was largely ascribed to its DNA binding capabilities leading to DNA fragmentation.[48] The literature trend suggests that the anticancer activities of **1–3** could closely linked to its groove-binding capabilities. Similarly, $[RuCl_2(PPh_3)L^b]$ (HL^b = 3-(benzothiazol-2-yliminomethyl)-phenol) afforded an IC_{50} value of 44.57 μM against MCF-7 cells which was attributed to the distinctive hyperchromism of the ligand-based electronic transition observed during its CT-DNA binding titrations which is synonymous with denaturation of the DNA double helix structure.

Generally, the IC_{50} values of the metal complexes described in this study fall in the low micromolar range in the three cancer cell lines tested, but it is evident that the metal complexes exhibit diverse cytotoxicity profiles. In particular, metal complex **1** is the least cytotoxic of the three compounds towards the non-cancerous MCF12-A cells. Their diversity in terms of anticancer activities are further emphasized by the fact that **1** displays the highest cytotoxicity against the MCF-7 breast cancer cell line, followed by the HeLa cervical cancer cell line, and is more than 10-fold less cytotoxic towards the HCC70 TNBC cell line compared to the MCF-7 receptor positive breast cancer cell line. On the other hand, **2** is more cytotoxic towards the HeLa cell line, while **3** displays similar cytotoxicity against all three cancer cell lines.

Time-dependent stability studies

UV-Vis absorption spectrophotometry was used to evaluate the chemical stabilities of **1**–**3** in solution, see Figures S21–S33. Although the UV-Vis spectra of the metal complexes in different media are comparable, the minor variations in their corresponding electronic transitions are attributed to the "solvent effect"..[49] Firstly, the electronic spectra of the respective metal complexes were monitored in anhydrous DMSO to assess their chemical stabilities in this organic solvent.

After 1 hour, noticeable alterations in the electronic spectrum of **1** are observed, see Figure S21. In particular, a disappearance of its π–π* intraligand transition which originally occurred at 272 nm was observed. There was an electron density redistribution of the intraligand transitions from 372 nm to 358 nm. The aforementioned electronic spectral changes are accompanied by a blue shifted decrementing LMCT band from 472 nm to 462 nm. At data collection intervals (t > 1 hr), gradual hypochromism of the new absorption bands appears followed by the emergence of a new ligand-based electronic transition at 347 nm. These UV-Vis spectral changes led to four distinct isosbestic points at 309 nm, 351 nm, 389 nm and 426 nm, respectively

Similarly, the overlay electronic spectra of **2** show minor blue-shifts of the intraligand and LMCT bands, see Figure S22. In the case of 3, a blue-shifted and decreasing MLCT band at 525 nm and an emerging MLCT band at 437 nm is bridged by a well-defined isosbestic point, see Figure S23. Also, a concurrent increase of the intraligand absorption band at 325 nm was observed. These alterations within the individual overlay UV-Vis spectra of **1–3** are accounted to ligand exchange between their chloro co-ligands and the DMSO solvent molecules due to the high nucleophilicity of its sulfur donor atom.

To indirectly corroborate if the chloride co-ligands was being substituted directly by the DMSO (*vide supra*), the electronic spectra of the respective metal complexes in DMSO and in the presence of excess anhydrous LiCl were monitored for 24 hrs at hourly intervals, see Figures S24–S26. Comparative UV-Vis spectral analysis revealed that the chloride substitution from the metal complexes was supressed. This was attributed to the common ion effect of the chloride ions since they were in excess-fold of the concentration of the Ru complexes in the DMSO solutions.

Consequently, the DMSO derivatives of **1**–**3** were formed at lower rates. The ligand exchange equilibrium remained largely to the left for all cases. The suppressed substitution rates of **1**–**3** in excess chloride concentrations are simulative of the bloodstream (100-110 mM) which proves that these chloro complexes are indeed kinetically stable in the aqueous medium, Scheme S1.

To further ascertain if the electronic spectral changes observed (*vide supra*) for these chloro ruthenium complexes under anhydrous conditions were due to the direct substitution of the chloride co-ligands by the DMSO solvent molecules, time-dependent stability studies were performed in the non-coordinative solvent, dichloromethane. The results were conclusive in that no similar electronic spectral modifications occurred, see Figures S28–S30. However, when the experiments were conducted in a 2% DMSO (v/v) with 98% aqueous polyphosphate buffer, minor changes in the different overlay UV-Vis spectral profiles are observed, see Figures S31–S33. This implied that **1–3** was kinetically stable against hydrolysis of the choro co-ligands by the water molecules of the aqueous buffer. Consequently, the DMSO molecules could not substitute the chloro ligands at a similar rate to what was observed in anhydrous DMSO. This further supports the kinetic stability of **1–3** under aqueous conditions. It is important to note that, in the cell biological (cytotoxicity) and molecular biological (DNA binding and Topo I inhibition) assays presented here, the DMSO concentration did not exceed 0.5% (v/v) in an aqueous environment.

Kinetic stability is an important parameter in the field of drug design and the resultant lability of the Ru–Cl bond of compounds **1**–**3** is a favourable aspect. It is a well-known fact that ruthenium complexes may serve as pro-drugs ("activation-by-reduction" hypothesis), where they are potentially reduced to their active form in the hypoxic tumour-cell environment while sparing normal cells from the toxic effects. The similar transport mechanisms to ferric ions of ruthenium anticancer agents in combination with redox activation in the hypoxia condition of the cancer cells may be responsible for their unique mechanisms of action as well a lower toxicity and fewer side effects of ruthenium anticancer agents.[50] Typically, these prodrugs contain labile ligands, such as chloride co-ligands, that can exchange with the donor atoms of the biological targets to form metal-biomolecule adducts. These resulting physical alterations define the general mechanism of biological activity for most of the metal complexes against cancer cells.[51]

Conclusion

This research study demonstrates the stabilization of the *trans*-$[Ru(PPh_3)_2]^{3+/2+}$ core by tridentate thiosemicarbazones and bidentate benzothiazole imines. The crystal structures of **1** and **2** depicted a rare tautomeric form of the chelating ligands, which is unique to monomeric ruthenium compounds while the neutral btm moiety in **3**, coordinates *via* its N_{imino} $N_{benzothiazole}$ donor set. Various spectral characterization techniques were used to confirm the structural elucidations of the metal complexes. Voltammograms of the metal compounds were dominated by metal-based redox transformation and the paramagnetic ruthenium compounds exhibited superior radical scavenging activities. DNA binding capabilities of the metal complexes were corroborated by AGE experiments using *g*DNA. In addition, methylene blue competition assays revealed that **1** and **2** were potential DNA intercalators. Compounds **1**–**3** were also demonstrated to act as topoisomerase I inhibitors by interfering with nicking of plasmid DNA *via* AGE. BSA interactions monitored by fluorescence and UV-Vis spectrophotometric titrations, showed that the metal compounds interact non-discriminately within the protein's hydrophobic cavities. Anticancer studies revealed that, in general, the metal complexes display selectivity for cancer cells compared to non-cancerous cells and rendered IC_{50} values in the low micromolar range against the cancer cell lines. Literature trends suggest the presence of the pharmacophores within the Schiff base chelators of **1**–**3** led to diverse cytotoxicity profiles in selected cancerous cells compared to other ruthenium Schiff base or heterocyclic compounds containing triphenylphosphine co-ligands. Time-dependent stability studies showed that in the presence of highly nucleophilic S-containing species such as DMSO, the chloride co-ligands of **1**–**3** can be substituted rapidly by the former. However, the complexes are quite stable in DCM or an aqueous phosphate buffer (pH 7.4) containing DMSO as minor component (2%). Their biotransformation is likely to occur selectively via the redox activation in the hypoxic environment of the cancer cells within a tumour This may enhances their therapeutic targeting and cytotoxicity.(, This may be a favourable characteristic for drug design.

Experimental Section

Materials and methods

The Schiff bases: Hpmt, Htmc and btm were synthesized according to literature methods.[52] The organic precursors, thiosemicarbazide, pyridine-2-carboxaldehyde, thiophene-2-carboxaldehyde, 5-amino-1-pentanol, benzothiazole-2-carboxaldehye as well as the metal precursor, *trans*-$[RuCl_2(PPh_3)_3]$ were obtained from Sigma-Aldrich. All solvents used were purchased from Merck SA and used without further purification. Electrochemical analysis grade tetrabutylammonium hexafluorophosphate, sodium nitroprusside, Griess reagent, high purity ascorbic acid, 2,2-diphenyl-1-picrylhydrazyl (DPPH), BSA, calf thymus (CT)-DNA, recombinant human topoisomerase I, phosphate buffered saline (PBS) tablets, ibuprofen and warfarin were also obtained from Sigma-Aldrich.

Melting point ranges were recorded with the aid of a Stuart SMP3 melting point device. Fluorescence measurements were conducted using a Perkin Elmer LS-45 fluorescence spectrometer fortified with a xenon lamp source and a 1 cm quartz emission cell. Electronic spectra were run on a Perkin-Elmer Lambda 25 where solid-state infrared spectra were recorded by means of a Perkin-Elmer Spectrum 100. NMR-grade solvent, d_6-DMSO (deuterated dimethyl sulfoxide) was used during the collection of NMR spectra with a Bruker Advance 400 MHz spectrometer equipped with an autosampler. Electrochemical grade tetrabutylammonium hexafluorophosphate (0.1 M) was added as a supporting electrolyte to the 2 mM dichloromethane solutions of the metal complexes. The investigation of their redox properties was performed using a Metrohm Autolab potentiostat in amalgamation with a three-electrode system: an auxiliary Pt counter electrode, a pseudo Ag|AgCl reference electrode and a glassy carbon working electrode (GCWE). The ESR spectra were collected using a Bruker EMX Ultra X spectrometer.

Synthesis of trans-P-[RuCl(PPh_3)$_2$(pmt)]Cl (1)

A 1:1 molar reaction of Hpmt (0.0188 g, 104 mmol) and *trans*-$[RuCl_2(PPh_3)_3]$ (0.100 g, 0.104 mmol) was heated until reflux for 3 hours in ethanol (20 cm^3). The brick-red solution was cooled to room temperature and a shiny brown precipitate filtered. The brown precipitate was dissolved in dichloromethane and placed in a diffusion chamber with hexane in the adjacent chamber. After several days, rectangular XRD quality crystals were afforded. Yield: 51%, m.p: 203.4–205.0 °C. IR (ν_{max}/cm^{-1}): υ(N–H) 3468 (w), 3049 (br, m); $\upsilon(C{=}N)_{thiolate}$ 1586 (w); $\upsilon(C{=}N)_{imino}$ 1552 (m); $\upsilon(C{-}N)_{thiolate}$ 1431 (s); $\upsilon(N{-}N)_{thiolate}$ 1088 (s); υ(Ru-[PPh_3]$_2$) 691 (s), 742 (vs). UV-Vis (DCM, ε, $M^{-1}\,cm^{-1}$): 282 nm (1730); 311 nm (1350); 368 nm (830); 481 nm (620); 680 nm (sh, 70). Anal. Found: C, 57.93; H, 4.39; N, 6.16; S, 1.70. Anal. Calcd (with 1 molecule of DCM): C, 57.54; H, 4.40; N, 5.96; S, 3.41.

Synthesis of trans-P-[RuCl(PPh_3)$_2$(tmc)]Cl (2)

A mixture of Htmc (0.0193 g, 104 mmol) and *trans*-$[RuCl_2(PPh_3)_3]$ (0.100 g, 0.104 mmol) in ethanol (20 cm^3) was heated until reflux for 3 hours. The resulting brown precipitate was filtered by gravity, dissolved in dichloromethane and placed in a diffusion chamber with hexane. After a few days, brown rectangular crystals which were suitable for X-ray analysis, were obtained. Yield: 47%. m.p:

222–226 °C. IR (ν_{max}/cm^{-1}): υ(N–H) 3353 (br, m), 3048 (w); υ(C=N)$_{thiolate}$ 1608 (m); υ(C=N)$_{imino}$ 1579 (s); υ(C–N)$_{thiolate}$ 1431 (s); υ(C=N)$_{thiolate}$ 1090 (s); υ(Ru-[PPh$_3$]$_2$) 694 (s), 742 (vs). UV-Vis (DCM, ε, M^{-1} cm^{-1}): 266 nm (3660); 329 nm (1070); 359 nm (1100); 447 (410); 589 nm (sh, 60). Anal. Found: C, 55.85; H, 4.23; N, 4.52; S, 4.11. Anal. Calcd (with 2 molecules of DCM): C, 55.52; H, 4.12; N, 4.52; S, 4.11.

Synthesis of cis-Cl, trans-P-[RuCl$_2$(PPh$_3$)$_2$(btm)] (3)

The title compound was formed from the equimolar reaction between btm (0.0259 g, 104 mmol) and *trans*-[RuCl$_2$(PPh$_3$)$_3$] (0.100 g, 0.104 mmol) after 3 hours of heating at reflux temperature in 20 cm^3 methanol. The resulting maroon solution was filtered, cooled to room temperature and allowed to stand at STP. X-ray quality cubic-shaped crystals were grown from the slow evaporation of the mother liquor. Yield: 33%, m.p: 280.7–284.0 °C. IR (ν_{max}/cm^{-1}): υ(O–H) 3461 (br, m); υ(C=N)$_{imino}$ 1534 (m); υ(C=N)$_{benzothiazole}$ 1479 (m); υ(C–N)$_{benzothiazole}$ 1429 (s); υ(Ru-[PPh$_3$]$_2$) 691 (s), 739 (vs). ^{1}H NMR (295 K/d^6 – CD$_6$SO/ ppm): 8.19 (1H, d, *H5*); 8.04 (1H, d, *H2*); 7.50–7.10 (33H, m, *2×PPh$_3$, H3, H4, H8*); 4.35 (1H, s, *OH*); 1.50–1.43 (2H, m, *H13, H13′, H12, H12′*); 1.50–1.05 (6H, m, *H11, H11′, H10, H10′, H9, H9′*). ^{31}P NMR (295 K/d_6 – CD$_6$SO/ ppm): 26.39. UV-Vis (DCM, ε, M^{-1} cm^{-1}): 282 nm (4340); 344 nm (sh, 740); 390 nm (sh, 160); 531 nm (840). Anal. Found: C, 62.34; H, 4.85; N, 2.92; S, 1.77. Anal. Calcd: C, 62.28; H, 4.91; N, 2.96; S, 3.39.

X-Ray diffraction

X-ray crystallographic data of the respective metal complexes was collected using a Bruker Apex Duo equipped with an Oxford Instruments Cryojet, which were operated at variable temperatures [100(2) K for **1**.(CH$_2$Cl$_2$), 293(2) K for **2**.2CH$_2$Cl$_2$ and **3**.CH$_3$OH] and an Incoatec microsource running at 30 W power. The details of the crystal structure refinement are summarized in Table 5 while the geometrical parameters are given in Table 6. X-ray radiation were induced with MoKα with a wavelength of 0.71073 Å. A mutual crystal-to-detector distance of approximately of 50 mm during radiation exposure.

Other instrumental conditions include phi and omega scans with exposures taken at 30 W X-ray power and 0.50° frame widths with APEX2.[53] The data processing was conducted by firstly using the SAINT program to reduce the data set by implementing standard Lorentz and polarization correction factors, scan speed scaling as well as outlier rejection.[53] Afterwards, SADABS semi-empirical multi-scan absorption correction[54] was applied which served as correction of the data. The structures were solved by making use of direct methods, WinGX[55] and SHELX-2016.[56] Subsequently, the non-hydrogen atoms were found by means of the difference density map and anisotropically refined with SHELX-2016.[56] All hydrogen atoms were defined as idealized contributors in the least squares process. A standard riding model were used to determine the hydrogen positions where the following parameters were used with C–H$_{methyl}$ distances of 0.98 Å, $U_{iso} = 1.5\ U_{eq}$, C–H$_{methylene}$ distances of 0.99 Å, $U_{iso} = 1.2\ U_{eq}$, C–H$_{aromatic}$ distances of 0.93 Å and $U_{iso} = 1.2\ U_{eq}$.

Antioxidant studies

Experimental procedures for the radical scavenging measurements were performed according to literature methods.[57] Experiments were conducted in triplicate to safeguard reproducibility of the data. The customary equation (**1**) was used to determine the experimental percentage radical scavenging activities:

$$\%\ Radical\ scavenging\ activity = \left(\frac{A_c - A_f}{A_c}\right) x\ 100 \qquad (1)$$

In equation (**1**), A_c is the absorbance of the control (DPPH or NO radicals) and A_f is the absorbance following the addition of the

Table 5. Crystal data and structure refinement data for metal compounds **1–3**.

Compound	**1**·(CH$_2$Cl$_2$)	**2**·2(CH$_2$Cl$_2$)	**3**·CH$_3$OH
Chemical formula	C43H38ClN4P2RuS·2(CH2Cl2)·Cl	C$_{42}$H$_{36}$ClN$_3$P$_2$RuS$_2$·2(CH$_2$Cl$_2$)·Cl	C$_{49}$H$_{46}$Cl$_2$N$_2$OP$_2$RuS·CH$_4$O
Formula weight	1046.59	1050.62	976.89
Temperature (K)	100(2)	293(2)	100(2)
Crystal system	Orthorhombic	Monoclinic	Monoclinic
Space group	*Ima2*	*Cc*	*P2$_1$*
Unit cell dimensions (Å, °)	$a = 22.7541(18)$	$a = 24.665(5)$	$a = 11.6529(6)$
	$b = 20.8853(15)$	$b = 20.590(2)$	$b = 11.1307(8)$
	$c = 9.6321(7)$	$c = 9.6333(10)$	$c = 12.4983(6)$
	$\alpha = 90$	$\alpha = 90$	$\alpha = 90$
	$\beta = 90$	$\beta = 111.074(4)$	$\beta = 113.447(2)$
	$\gamma = 90$	$\gamma = 90$	$\gamma = 90$
Crystal size (mm)	0.24×0.15×0.09	0.33×0.19×0.11	0.14×0.11×0.09
V (Å^3)	4577.4(6)	4565.1(8)	2288.9(2)
Z	4	4	2
Density (calc.) (Mg/m^3)	1.517	1.529	1.417
Absorption coefficient (mm^{-1})	0.85	0.89	0.62
F (000)	2124	2136	1008
Θ range for data collection (deg)	2.65°; 28.10°	2.65°; 28.23°	2.97°; 27.22°
Index ranges	$-30 \le h \le 30$	$-32 \le h \le 32$	$-14 \le h \le 14$
	$-27 \le k \le 27$	$-27 \le k \le 27$	$-18 \le k \le 21$
	$-12 \le l \le 12$	$-12 \le l \le 12$	$-15 \le l \le 15$
Reflections measured	11493	11323	17785
Observed reflections ($I > 2\sigma(I)$)	5800	5668	8335
Independent reflections	3973	5512	6880
Data/ restraints/parameters	4075/1/295	4951/2/527	8335/56/563
Goodness of fit on F^2	1.13	1.07	1.05
Observed R; wR^2	0.023; 0.062	0.033; 0.107	0.049; 0.124
R_{int}	0.022	0.033	0.046

Table 6. Selected bond lengths [Å] and angles [°] for **1**.

1		2		3	
Ru–Cl1	2.4289(11)	Ru–Cl1	2.421(1)	Ru–Cl1	2.435(2)
Ru–P1	2.3788(7)	Ru–P1	2.399(1)	Ru–Cl2	2.448(2)
Ru–P2	2.3788(7)	Ru–P2	2.393(1)	Ru–N1	2.089(6)
Ru–S	2.3812(12)	Ru–S1	2.383(1)	Ru–N2	2.010(7)
Ru–N1	2.101(4)	Ru–S2	2.345(1)	Ru–P1	2.402(2)
Ru–N2	1.970(4)	Ru–N1	2.039(4)	Ru–P2	2.387(3)
N1–C1	1.337(6)	C6–S2	1.705(5)	C7–N1	1.333(9)
N1–C5	1.338(6)	C1–S1	1.714(5)	C6–N1	1.40(1)
C6–N2	1.305(6)	C4–S2	1.721(5)	C8–N2	1.30(1)
N2–N3	1.368(6)	C5–N1	1.298(7)	C7–S	1.726(8)
C7–N3	1.357(6)	N1–N2	1.380(6)	C1–S	1.724(9)
C7–N4	1.331(6)	C6–N2	1.325(7)	P1–Ru–P2	177.05(8)
C7–S	1.703(5)	C6–N3	1.345(6)	Cl1–Ru–Cl2	90.17(7)
P1–Ru–P2	173.26(4)	S1–Ru–S2	160.01(4)	Cl1–Ru–N1	100.2(2)
N2–Ru–S	83.19(12)	N1–Ru–Cl1	177.8(1)	Cl2-Ru–N2	91.59(2)
N2–Ru–N1	77.74(15)	N1–Ru–S2	78.7(1)	N1–Ru–N2	78.2(3)
N2–Ru–Cl1	178.42(12)	N1–Ru–S1	82.2(1)	–	–
N1–Ru–S	160.93(10)	P1-Ru–P2	175.46(4)	–	–

individual metal compounds to the control. The characteristic experimental percentage radical scavenging activities was then used to calculate the IC_{50} values (concentrations that induce 50% radical scavenging activity) of **1–3**. The DPPH radical assay was performed by measuring the UV-Vis spectrum of the control [DPPH (0.2 mM in MeOH)] followed by the addition of 1 mL of a metal compound [30 μM in MeOH] and then, to ensure homogeneity, the sample was shaken. Incubation times of 20 minutes in the dark was applied for each sample solution before their respective UV-Vis spectra were collected.

The following experimental procedure was used for the nitric oxide (NO) radical assay: initially, preparation of a 10 mM solution of sodium nitroprusside was carried out in PBS buffer and incubated at room temperature for 3 hours. Subsequently, the control was prepared by adding Griess reagent (1 cm^3) to a 0.5 cm^3 of the nitroprusside solution followed by the collection of its UV-Vis spectrum. Sample preparations included the addition of a metal compound (30 μM in MeOH) to a 0.5 cm^3 aliquot of sodium nitroprusside. Following an incubation time of 3 hours, 1 cm^3 of Griess reagent was added to each sample solution and its individual UV-Vis spectra were run.

DNA binding ability of the complexes

To assess the ability of the compounds to competitively bind to genomic DNA (gDNA) to displace ethidium bromide (EtBr), agarose gel electrophoresis (AGE) was performed, as previously reported by Gramni, et al., 2019.[58] The compounds (50 μM and 200 μM), DMSO [2% (v/v)] or cisplatin (200 μM) were incubated with 100 ng of gDNA (total reaction volume of 20 μL) for 4 hours at 37 °C. Subsequently, 13 μL reaction mixture and 2 μL of 6× loading dye was loaded onto a 0.8% (w/v) agarose gel containing 0.5 μg/ml Ethidium Bromide. The gel was electrophoresed for 45 minutes at 90 V in 1 X Tris-acetic acid EDTA (TAE: 40 mM Tris- acetate, 1 mM EDTA). The resulting bands were detected using a ChemiDoc XRS System (Bio-Rad Laboratories) with Image Lab Software (Bio-Rad Laboratories).[59]

To determine whether the compounds competitively bound to calf thymus DNA by intercalation, the methylene blue DNA competition assay was utilised.[30,60] A reaction mixture containing 15 μg/ml methylene blue dye (a minor groove binder), fixed concentration of 100 ng calf thymus DNA (ctDNA), the respective complexes (50 μM and 200 μM) and MilliQ water were added in a final 100 μL reaction volume to a clear bottomed black-walled 96-well plate. The reaction mixture was incubated at room temperature in the dark for 10 minutes. The fluorescence was then measured on a Spectramax spectrophotometer (Molecular Devices, USA) at an excitation wavelength of 665 nM and emission wavelength range of 650 to 690 nM in 5 nM intervals.[60b] The experiment was performed in triplicate and the data was analysed using GraphPad Prism Inc, (USA).

Topoisomerase I inhibition study

In order to determine whether the compounds affected the ability of the enzyme Topoisomerase I (Topo I) to relax supercoiled DNA, a Topo I inhibition study was performed. The Topo I assay was adapted according to Kadioglu (2017).[32] The reaction mixture contained 1 μL plasmid pcDNA-CL8D-HisCYP2 A6 (215 ng), 2 μL of 5× reaction buffer (50 mM Tris-HCl pH 7.5, 50 mM KCl, 10 mM $MgCl_2$, 0.5 mM DTT, 0.1 mM EDTA and 30 μg/ml BSA), 2 Units of Topo 1 enzyme, 1 μL of the compounds **1**–**3** (50 μM and 200 μM) and MilliQ water to make up a reaction final volume of 10 μL. The reaction mix was incubated at room temperature for 15 minutes and 2 μL of 6× loading dye was added. The entire volume of 12 μL was then loaded onto a 0.6% agarose gel without ethidium bromide (EtBr) and electrophoresed in TAE buffer. A sample of the plasmid digested with the single cutter HindIII was also loaded in order to visualize the linearized digested plasmid DNA as a means of comparison and to confirm the supercoiled conformation. The untreated supercoiled pcDNA-CL8D-HisCYP2A6 plasmid was loaded as a negative control and camptothecin (200 μM) was included as a positive control. The gel was then stained with 50μg/ml of EtBr for 20 min and washed twice with ddH_2O. It was then visualized under UV light using a ChemiDoc XRS System (BIO-RAD, USA).

BSA binding interaction studies

PBS buffer at a pH of 7.2 was used to prepare the BSA stock solution. BSA concentration was ascertained spectrophotometrically by means of an extinction coefficient of 43824 $M^{-1}cm^{-1}$ at 280 nm.[61] All stock solutions were prepared in MeOH.

The BSA interaction studies were performed by maintaining the BSA concentration (~20 μM) whilst varying the concentrations of the respective metal compounds (0–~380 μM). Two-minute incubation periods were utilized for each sample mixture. Equivalent

volumes of metal compound were added to both the reference and sample cells. The absorption titration data was fitted to the following equation:

$$\left[\frac{A_o}{A_o - A}\right] = \left(\frac{\varepsilon_{BSA}}{\varepsilon_B}\right) + \left(\frac{\varepsilon_{BSA}}{\varepsilon_B . k_{app}}\right). \left(\frac{1}{C_{compound}}\right) \quad (2)$$

In equation (**2**), A_0 and A are the absorbance values of BSA at 280 nm in the absence and presence of a metal compound, ε_{BSA} and ε_B are the extinction coefficients of BSA and the bound metal complex respectively (*viz.* adduct of a metal compound and BSA), k_{app} is equivalent to the apparent association constant and $C_{compound}$ is the concentration of a metal compound. The following double reciprocal plot can be produced from equation (**2**) and the apparent association constant (k_{app}) is determined from the ratio of the intercept to the slope.[62]

$$\frac{1}{(A_o - A)} \; vs \; \left(\frac{1}{C_{complex}}\right)$$

The influence upon increasing the concentrations of the metal compounds on the emission spectrum of BSA were studied. Fluorescence emission spectra were performed at a temperature of 293 K with the width of emission and excitation slits adjusted to 5 nm. A wavelength range of 300–500 nm at an excitation wavelength of 280 nm were utilized in the running of the emission spectra. Using the Stern-Volmer relationship,[63] data obtained was used to estimate the Stern-Volmer quenching constant (K_{SV}):

$$\frac{I_0}{I} = 1 + K_{SV} \; [complex] \quad (3)$$

Where I_0 and I are the emission intensities in the absence and presence of the metal compounds. The K_{SV} values were obtained from the slope of the plot:

$$\frac{I_0}{I} \; vs \; [complex]$$

Subsequently, the quenching rate constant (k_q) could be obtained from equation (**4**):

$$K_{SV} = k_q \; \tau_0 \quad (4)$$

Where τ_0 is the lifetime of the protein (10^{-8} s) without a quencher.

Data correction was applied to the quenching titration studies to compensate for the inner filter effect using equation (**5**) (Nehru et al., 2020):

$$F_{COR} = F_{OBS} \times 10^{(A_1 + A_2)/2}, \quad (5)$$

where, F_{COR} and F_{OBS} are designated as the corrected and observed fluorescence intensities, respectively, whereas A_1 and A_2 are defined as the absorbance values of each ratio of BSA and a metal complex at peak maxima of the excitation and emission wavelengths, respectively.

Competitive binding studies were conducted using two distinct site markers (competitors), *viz.*, Warfarin for site **I** and Ibuprofen for site **II**. Initially, an equimolar amount of the competitor was added to the BSA (each at 5 μM) and any variations in the fluorescence spectra were noted. The fluorescence titration was then achieved by varying the concentration of the metal compounds in the BSA-competitor solution and noting any spectral changes.[64] Data from the titrations once again were fitted to the Stern-Volmer plot (equation **3**) and the resulting rate and quenching constants were compared to those in the absence of the competitors.[65]

In vitro anti-cancer studies

The cytotoxicity of the **1**–**3** was evaluated against the HeLa cervical cancer cell line, HCC70 triple negative breast cancer cell line, MCF-7 hormone responsive breast cancer cell line and a non-tumorigenic breast epithelial cell line MCF12A. Paclitaxel, a known chemotherapeutic agent for various cancers,[66] was also tested and used as a control. Cytotoxicity and IC_{50} values were determined by the resazurin assay according to the method described in Mbaba.[60b] The cells were seeded at a density of 5000 cells/ well and allowed to attach overnight in an incubator at 37 °C and 9% CO_2. Subsequently, the cells were treated with the **1**–**3** (concentration range 15.63 to 500.00 μM), vehicle control (2% (v/v) DMSO) or the positive control paclitaxel (0.16 to 500 nM) for 96 hours at 37 °C in a 9% CO_2 incubator. After 96 hrs exposure, 0.54 nM of resazurin solution was added and the cells were incubated for 2–4 hours at 37 °C in a 9% CO_2 incubator. The fluorescence was then measured on a Spectramax spectrophotometer (excitation and emission wavelength set at 560 nm and 590 nm, respectively). The experiment was performed in triplicate and the data was analyzed using GraphPad Prism Inc, (USA) with half-maximal inhibitory concentration (IC_{50} values) determined by non-linear regression. Selectivity indexes of the compounds were calculated as follows: (IC_{50} value in MCF12-A)/(IC_{50} value in cancer cell line). A selectivity index >1 indicates selectivity for cancer cells over non-cancerous cells.

Crystallography data

CCDC 1952019–1952021 contains the supplementary crystallographic data for this paper. These data can be obtained free of charge from The Cambridge Crystallographic Data Centre *via* www.ccdc.cam.ac.uk/data_request/cif.

Time-dependent stability studies

In DMSO: Compounds **1**–**3** were dissolved in anhydrous DMSO (10^{-5} M) at room temperature and filtered. The UV-Vis spectra were recorded at 1 hour intervals for 24 hours.

In DMSO with saturated LiCl: DMSO solutions of compounds **1**–**3** (10^{-5} M) were prepared as described from above, (10^{-5} M) were saturated with excess amounts of LiCl at room temperature and then filtered. The UV-Vis spectra were then run of each individual compound 1 hour intervals for 23 hours at 310 K.

In DCM: Fresh solutions of compounds **1**–**3** were prepared at room temperature (10^{-5} M) and then filtered. The UV-Vis spectra were documented at 1 hour intervals for 23 hours at 310 K.

In the simulated biological medium: Due to the solubility of the compounds, they were dissolved in a 2% (v/v) DMSO solution (98% polyphosphate buffer) at room temperature and the pH adjusted to 7.2, thereafter UV-Vis spectra were run at 1 hour intervals for 14 hours at 310 K.

Acknowledgements

This research was supported by funding from the Thuthuka NRF (Research Grant No. 94020 and 190403426633), Incentive Funding for Rated Researchers NRF (Research Grant No. 114737), University of KwaZulu-Natal and Rhodes University. The views expressed are those of the authors and should not be attributed to the NRF or University of KwaZulu-Natal.

Conflict of Interest

The authors declare no conflict of interest.

Data Availability Statement

The data that support the findings of this study are available from the corresponding author upon reasonable request.

Keywords: Ruthenium · thiosemicarbazone · benzothiazole · biomolecular interactions · cytotoxicity

[1] U. Ndagi, N. Mhlongo, M. E. Soliman, *Drug Des. Dev. Ther.* **2017**, *11*, 599–616.
[2] A. Notaro, G. Gasser, *Chem. Soc. Rev.* **2017**, *46*(23), 7317–7337.
[3] L. Zeng, P. Gupta, Y. Chen, E. Wang, L. Ji, H. Chao, Z.-S. Chen, *Chem. Soc. Rev.* **2017**, *46*(19), 5771–5804.
[4] P. Kumar, S. Swagatika, S. Dasari, R. S. Tomar, A. K. Patra, *J. Inorg. Biochem.* **2019**, *199*, 110769.
[5] a) M. M. Kasprzak, L. Szmigiero, E. Zyner, J. Ochocki, *J. Inorg. Biochem.* **2011**, *105*(4), 518–524; b) M. Kubanik, W. Kandioller, K. Kim, R. F. Anderson, E. Klapproth, M. A. Jakupec, A. Roller, T. Sohnel, B. K. Keppler, C. G. Hartinger, *Dalton Trans.* **2016**, *45*(33), 13091–13103; c) Z. Wang, H. Qian, S.-M. Yiu, J. Sun, G. Zhu, *J. Inorg. Biochem.* **2014**, *131*, 47–55.
[6] a) A. Rouf, C. Tanyeli, *Eur. J. Med. Chem.* **2015**, *97*, 911–927; b) S. Sardari, S. Feizi, A. H. Rezayan, P. Azerang, S. Mohammad Shahcheragh, G. Ghavami, A. Habibi, *Iran. J. Pharm. Res.* **2017**, *16*(3), 1128; c) S. Singhal, S. Arora, S. Agarwal, R. Sharma, N. Singhal, *World. J. Pharm. and Pharm. sci.* **2013**, *2*, 4661–4681.
[7] a) M. Richert, M. Walczyk, M. J. Cieślak, J. Kaźmierczak-Barańska, K. Królewska-Golińska, G. Wrzeszcz, T. Muzioł, S. Biniak, *Dalton Trans.* **2019**, *48*(28), 10689–10702; b) K. Sampath, S. Sathiyaraj, C. Jayabalakrishnan, *Spectrochim. Acta Part A* **2013**, *105*, 582–592.
[8] C. B. Spillane, N. C. Fletcher, S. M. Rountree, H. van den Berg, S. Chanduloy, J. L. Morgan, F. R. Keene, *Journal of biological inorganic chemistry : JBIC : a publication of the Society of Biological Inorganic Chemistry* **2007**, *12(6)*, 797–807.
[9] H. Yildirim, E. Guler, M. Yavuz, N. Ozturk, P. Kose Yaman, E. Subasi, E. Sahin, S. Timur, *Mater. Sci. Eng. C* **2014**, *44*, 1–8.
[10] P. Mishra, M. Jha, R. C, C. Kumar, *Synthesis and Characterization of Divalent Transition Metal Complexes Containing Thiosemicarbazone Ligands*, **2013**.
[11] P. Novak, K. Pičuljan, T. Biljan, T. Hrenar, M. Cindrić, M. Rubčić, Z. Meić, *Deuterium Isotope Effects in 13 C NMR Spectra of Intramolecularly Hydrogen-Bonded Salicylaldehyde-4-phenylthiosemicarbazone*, **2007**.
[12] M. Maji, P. Sengupta, S. K. Chattopadhyay, G. Mostafa, C. H. Schwalbe, S. Ghosh, *J. Coord. Chem.* **2001**, *54*(1), 13–24.
[13] a) T. Satyanarayana, K. V. Reddy, *Proceedings of the Indian Academy of Sciences - Chemical Sciences* **1987**, *99*(4), 237–242; b) H. L. Singh, J. Singh, A. Mukherjee, *Bioinorg. Chem. Appl.* **2013**, *2013*, 9.
[14] K. P. Balasubramanian, R. Karvembu, R. Prabhakaran, V. Chinnusamy, K. Natarajan, *Spectrochim. Acta Part A* **2007**, *68*(1), 50–54.
[15] a) R. Kumar, S. Kumar, M. Bala, A. Ratnam, U. Singh, K. Ghosh, *J. Organomet. Chem.* **2018**, *863*, 77–83; b) G. Kalaiarasi, S. R. J. Rajkumar, S. Dharani, F. R. Fronczek, R. Prabhakaran, *J. Organomet. Chem.* **2018**, *866*, 223–242.
[16] a) M. Al-Noaimi, F. F. Awwadi, B. Atallah, D. Taher, A. Hammoudeh, H. Lang, T. Rüffer, *Polyhedron* **2017**, *123*, 47–55; b) I. N. Booysen, A. Adebisi, M. P. Akerman, O. Q. Munro, B. Xulu, *J. Coord. Chem.* **2016**, *69*(10), 1641–1652.
[17] S. Singh, F. Athar, M. R. Maurya, A. Azam, *Eur. J. Med. Chem.* **2006**, *41*(5), 592–598.
[18] R. R. Kumar, R. Ramesh, J. G. Małecki, *Journal of Photochemistry and Photobiology B: Biology* **2016**, *165*, 310–327.
[19] S. A. Elsayed, S. Harrypersad, H. A. Sahyon, M. A. El-Magd, C. J. Walsby, *Molecules* **2020**, *25*(18), 4284.
[20] a) M. Fandzloch, A. Wojtczak, J. Sitkowski, I. Łakomska, *Polyhedron* **2014**, *67*, 410–415; b) M. Fandzloch, A. Wojtczak, J. Wiśniewska, K. Stefańczak, J. M. Salas, I. Łakomska, *Inorg. Chim. Acta* **2016**, *443*, 170–178.
[21] a) R. Prabhakaran, P. Kalaivani, R. Jayakumar, M. Zeller, A. Hunter, S. Renukadevi, E. Ramachandran, K. Natarajan, *Metallomics* **2011**, *3*(1), 42–48; b) R. Raveendran, S. Pal, *J. Organomet. Chem.* **2007**, *692*(4), 824–830.
[22] A. A. Batista, M. O. Santiago, C. L. Donnici, I. S. Moreira, P. C. Healy, S. J. Berners-Price, S. L. Queiroz, *Polyhedron* **2001**, *20*(17), 2123–2128.
[23] a) L.-H. Tang, X. Chen, A.-Q. Jia, Z. Xin, Q.-F. Zhang, *Inorg. Chim. Acta.* **2018**, *480*, 108–112; b) L.-H. Tang, F. Wu, H. Lin, A.-Q. Jia, Q.-F. Zhang, *Inorg. Chim. Acta.* **2018**, *477*, 212–218; c) J. Ji, X. Chen, H. Lin, A.-Q. Jia, Q.-F. Zhang, *Inorg. Chim. Acta.* **2019**, *494*, 105–111.
[24] a) P. Kalaivani, R. Prabhakaran, P. Poornima, F. Dallemer, K. Vijayalakshmi, V. V. Padma, K. Natarajan, *Organometallics* **2012**, *31*(23), 8323–8332; b) S. Datta, M. G. B. Drew, S. Bhattacharya, *Indian Journal of Chemistry - Section A Inorganic, Physical, Theoretical and Analytical Chemistry* **2011**, *50 A*, 1403–1409.
[25] a) A. Garza-Ortiz, P. U. Maheswari, M. Siegler, A. L. Spek, J. Reedijk, *New J. Chem.* **2013**, *37*(11), 3450–3460; b) I. N. Booysen, S. Maikoo, M. P. Akerman, B. Xulu, *Trans. Met. Chem.* **2015**, *40*(4), 397–404; c) L. C. Matsinha, P. Malatji, A. T. Hutton, G. A. Venter, S. F. Mapolie, G. S. Smith, *Eur. J. Inorg. Chem.* **2013**, *2013*(24), 4318–4328.
[26] Y. Lin, M. Jiang, W. Chen, T. Zhao, Y. Wei, *Biomed. Pharmacother.* **2019**, *118*, 109249.
[27] K. Neha, M. R. Haider, A. Pathak, M. S. Yar, *Eur. J. Med. Chem.* **2019**, *178*, 687–704.
[28] a) P. Srivastava, R. Mishra, M. Verma, S. Sivakumar, A. K. Patra, *Polyhedron* **2019**; b) M. Marques da Silva Paula, C. T. Pich, F. Petronilho, L. B. Drei, M. Rudnicki, M. Roberto de Oliveira, J. C. F. Moreira, J. A. P. Henriques, C. V. Franco, F. Dal Pizzol, *Redox report : communications in free radical research* **2005**, *10*(3), 139–143.
[29] a) C. Gürses, A. Aktaş, S. Balcıoğlu, A. Fadhilah, Y. Gök, B. Ateş, *J. Mol. Struct.* **2022**, *1247*, 131350; b) S. Maikoo, A. Chakraborty, N. Vukea, L. M. K. Dingle, W. J. Samson, J.-A. de la Mare, A. L. Edkins, I. N. Booysen, *J. Biomol. Struct.* **2021**, *39*(11), 4077–4088.
[30] P. Vardevanyan, A. Antonyan, M. Parsadanyan, M. Shahinyan, L. Hambardzumyan, *J. Appl. Spectrosc.* **2013**, *80*(4), 595–599.
[31] a) J. P. Hall, K. O'Sullivan, A. Naseer, J. A. Smith, J. M. Kelly, C. J. Cardin, *Proc. Natl. Acad. Sci. USA* **2011**, *108*(43), 17610–17614; b) V. Brabec, J. Kasparkova, *Coord. Chem. Rev.* **2018**, *376*, 75–94; c) A. E. Friedman, J. C. Chambron, J. P. Sauvage, N. J. Turro, J. K. Barton, *J. Am. Chem. Soc.* **1990**, *112*(12), 4960–4962.
[32] O. Kadioglu, A. Chan, A. Cong Ling Qiu, V. K. W. Wong, V. Colligs, S. Wecklein, H. Freund-Henni Rached, T. Efferth, W.-L. W. Hsiao, *Front. Pharmacol.* **2017**, *8*, 711.
[33] Y. Pommier, *Nat. Rev. Cancer* **2006**, *6*(10), 789–802.
[34] a) Y.-C. Wang, C. Qian, Z.-L. Peng, X.-J. Hou, L.-L. Wang, H. Chao, L.-N. Ji, *J. Inorg. Biochem.* **2014**, *130*, 15–27; b) X. He, L. Jin, L. Tan, *Spectrochim. Acta Part A* **2015**, *135*, 101–109.
[35] A. R. Simović, R. Masnikosa, I. Bratsos, E. Alessio, *Coord. Chem. Rev.* **2019**, *398*, 113011.
[36] a) Q. Zhang, Y. Ni, *RSC Adv.* **2017**, *7*(63), 39833–39841; b) M. Dieaconu, A. Ioanid, S. Iftimie, S. Antohe, *Digest Journal of Nanomaterials and Biostructures* **2012**, *7*, 1125–1138; c) V. D. Suryawanshi, L. S. Walekar, A. H. Gore, P. V. Anbhule, G. B. Kolekar, *J. Pharm. Anal.* **2016**, *6*(1), 56–63.
[37] Z. Chi, B. Hong, X. Ren, K. Cheng, Y. Lu, X. Liu, *Spectr. Lett.* **2018**, *51*(6), 279–286.
[38] a) M. Rajabi, M. A. Khalilzadeh, F. Tavakolinia, P. Signorelli, R. Ghidoni, E. Santaniello, *DNA Cell Biol.* **2012**, *31*(5), 783–789; b) R. Kumaran, P. Ramamurthy, *J. Fluoresc.* **2011**, *21*(4), 1499–1508.
[39] S. R. Hsieh, P. M. Reddy, C. J. Chang, A. Kumar, W. C. Wu, H. Y. Lin, *Polymers (Basel).* **2016**, *8*(6).

[40] a) Y. Sun, B. Su, Q. Xu, R. Liu, *Appl. Spectrosc.* **2012**, *66*(7), 791–797; b) S.-T. Li, Z.-Y. Ma, X. Liu, J. Tian, S.-P. Yan, *Synthesis, crystal structures, DNA/bovine serum albumin binding, DNA cleavage and cytotoxicity of five mononuclear zinc(II) complexes*, **2017**.
[41] Z. Tavsan, P. K. Yaman, E. Subasi, H. A. Kayali, *Journal of biological inorganic chemistry: JBIC: a publication of the Society of Biological Inorganic Chemistry* **2018**, *23*(3), 425–435.
[42] N. Sankar, J. Eswaran, T. Murugan, B. Nattamai, S. P. M. A. Neelakantan, K. M. Velusamy, *Appl. Organomet. Chem.* **2019**, e4751.
[43] a) P. Mandal, B. K. Kundu, K. Vyas, V. Sabu, A. Helen, S. S. Dhankhar, C. M. Nagaraja, D. Bhattacherjee, K. P. Bhabak, S. Mukhopadhyay, *Dalton Trans.* **2018**, *47*(2), 517–527; b) A. C. de Melo, J. M. Santana, K. J. Nunes, B. L. Rodrigues, N. Castilho, P. Gabriel, A. H. Moraes, M. d. A. Marques, G. A. de Oliveira, Í. P. de Souza, *Molecules* **2019**, *24*(11), 2154.
[44] T. Wybranowski, B. Ziomkowska, A. Cwynar, S. Kruszewski, *Opt. Appl.* **2014**, *44*, 357–364.
[45] Y. Chang-Qing, L. Jie, Z. Shi-Qi, Z. Kun, G. Zi-Qian, X. Ran, L. Hui-Meng, Z. Ren-Bin, Z. Gang, Y. Da-Chuan, *Progress in biophysics and molecular biology* **2020**, *151*, 40–53.
[46] D. P. Dorairaj, Y.-F. Lin, J. Haribabu, T. Murugan, M. Narwane, R. Karvembu, M. A. Neelakantan, C.-L. Kao, C.-C. Chiu, S. C. Hsu, *J. Inorg. Biochem.* **2021**, *223*, 111545.
[47] S. Maikoo, L. M. K. Dingle, A. Chakraborty, B. Xulu, A. L. Edkins, I. N. Booysen, *Polyhedron* **2020**, *184*, 114569.
[48] S. A. Elsayed, H. E. Badr, A. di Biase, A. M. El-Hendawy, *J. Inorg. Biochem.* **2021**, *223*, 111549.
[49] K. Yamaguchi, T. Murai, Y. Tsuchiya, Y. Miwa, S. Kutsumizu, T. Sasamori, N. Tokitoh, *RSC Adv.* **2017**, *7*(29), 18132–18135.
[50] R. G. Kenny, C. J. Marmion, *Chem. Rev.* **2019**, *119*(2), 1058–1137.
[51] A. Levina, P. A. Lay, *Inorg. Chem. Front.* **2014**, *1*(1), 44–48.
[52] a) D. Kovala-Demertzi, P. N. Yadav, J. Wiecek, S. Skoulika, T. Varadinova, M. A. Demertzis, *J. Inorg. Biochem.* **2006**, *100*(9), 1558–1567; b) W.-S. Hong, C.-Y. Wu, C.-S. Lee, W.-S. Hwang, M. Chiang, *J. Organomet. Chem.* **2004**, *689*, 277–285; c) M. B. Ismail, I. N. Booysen, M. P. Akerman, *Inorg. Chem. Commun.* **2017**, *78*, 78–81.
[53] *Bruker APEX2, SAINT and SADABS (2010). Bruker AXS Inc. Madison., Wisconsin, USA.*, Bruker AXS Inc. Madison, Wisconsin, USA.
[54] R. H. Blessing, *Acta Crystallogr A* **1995**, *51 (Pt 1)*, 33–38.
[55] L. Farrugia, *J. Appl. Crystallogr.* **2012**, *45*(4), 849–854.
[56] G. Sheldrick, *Acta Crystallogr. Sect. A* **2008**, *64*(1), 112–122.
[57] a) P. Krishnamoorthy, P. Sathyadevi, K. Senthilkumar, P. T. Muthiah, R. Ramesh, N. Dharmaraj, *Inorg. Chem. Commun.* **2011**, *14*(9), 1318–1322; b) R. Ramachandran, P. Viswanathamurthi, *Spectrochim. Acta Part A* **2013**, *103*, 53–61.
[58] L. Gramni, N. Vukea, A. Chakraborty, W. J. Samson, L. M. K. Dingle, B. Xulu, J.-A. de la Mare, A. L. Edkins, I. N. Booysen, *Inorg. Chim. Acta.* **2019**, *492*, 98–107.
[59] C. A. Schneider, W. S. Rasband, K. W. Eliceiri, *Nat. Methods* **2012**, *9*(7), 671–675.
[60] a) W.-Y. Li, J.-G. Xu, X.-W. He, *Anal. Lett.* **2000**, *33*, 2453–2464; b) M. Mbaba, L. M. Dingle, D. Cash, J.-A. de la Mare, D. Laming, D. Taylor, H. C. Hoppe, A. L. Edkins, S. D. Khanye, *Eur. J. Med. Chem.* **2020**, *187*, 111924.
[61] D. H. Atha, U. Manne, W. E. Grizzle, P. D. Wagner, S. Srivastava, V. Reipa, *J. Histochem. Cytochem.* **2010**, *58*(11), 1005–1014.
[62] W. Zhong, Y. Wang, J. S. Yu, Y. Liang, K. Ni, S. Tu, *J. Pharm. Sci.* **2004**, *93*(4), 1039–1046.
[63] T. Mukherjee, M. Mukherjee, T. K. Mondal, A. Moirangthem, A. Basu, E. Zangrando, P. Chattopadhyay, *J. Coord. Chem.* **2013**, *66*(15), 2747–2764.
[64] M. D. Meti, S. T. Nandibewoor, S. D. Joshi, U. A. More, S. A. Chimatadar, *J. Pharm. Anal.* **2015**, *5*(4), 249–255.
[65] N. Na, D.-Q. Zhao, H. Li, N. Jiang, J.-Y. Wen, H.-Y. Liu, *Molecules* **2015**, *21*(1), E54-E54.
[66] K. Priyadarshini, A. U. Keerthi, *Med. Chem.* **2012**, *2*(7), 139–141.

Manuscript received: August 12, 2022
Revised manuscript received: August 30, 2022
Accepted manuscript online: August 30, 2022
Version of record online: September 21, 2022